HHS Public Access

Author manuscript

*Science*. Author manuscript; available in PMC 2016 March 28.

Published in final edited form as:

*Science*. 2015 September 4; 349(6252): aaa4352. doi:10.1126/science.aaa4352.

# Neutrophil trails guide influenza-specific CD8+ T cells in the airways

**Kihong Lim**[1,*], **Young-Min Hyun**[1,*], **Kris Lambert-Emo**[1], **Tara Capece**[1], **Seyeon Bae**[1], **Richard Miller**[2], **David J. Topham**[1], and **Minsoo Kim**[1,§]

[1]Department of Microbiology and Immunology, David H. Smith Center for Vaccine Biology and Immunology, University of Rochester, Rochester, NY, USA

[2]Department of Pharmacology, Northwestern University, Chicago, IL, USA

## Abstract

During viral infections, chemokines guide activated effector T cells to infection sites. However, the cells responsible for producing these chemokines and how such chemokines recruit T cells is unknown. Here, we show that the early recruitment of neutrophils into influenza-infected trachea is essential for $CD8^+$ T cell-mediated immune protection in mice. We observed that migrating neutrophils leave behind long-lasting trails that are enriched in the chemokine CXCL12. Experiments with granulocyte-specific CXCL12 conditional knock-out mice and a CXCR4 antagonist revealed that CXCL12 derived from neutrophil trails is critical for virus-specific $CD8^+$ T cell recruitment and effector functions. Collectively, these results suggest neutrophils deposit long-lasting, chemokine-containing trails, which may provide both chemotactic and haptotactic cues for efficient $CD8^+$ T cell migration and localization in influenza-infected tissues.

---

The maintenance of homeostatic immune surveillance and the development of effective adaptive immune responses require that T cells cross tissue barriers and move throughout the body, migrating in and out of the bone marrow, lymphoid and non-lymphoid tissues, under both normal and infected or inflamed conditions (8). The efficient trafficking of activated effector T cells into peripheral non-lymphoid tissues is key to enact their protective functions. A successful early local innate immune response is critical for elicitation of T cell effector functions at the peripheral tissue sites (9). Therefore, it is likely that the type of innate cells, mode of early innate responses, and associated local inflammatory mediators will all impact on the molecular mechanisms by which effector T cells successfully move into the inflamed tissues.

---

§To whom correspondence should be addressed: Minsoo Kim, Ph.D., Department of Microbiology & Immunology, David H. Smith Center for Vaccine Biology and Immunology, University of Rochester Medical Center, 601 Elmwood Avenue, Box 609, Rochester, NY 14642, minsoo_kim@urmc.rochester.edu, Phone: (585) 276-3917, Fax: (585) 273-2452.

*These authors contributed equally to this work.

The data presented in this manuscript are tabulated in the main paper and in the supplementary materials. K.L. conducted most of the experiments and performed most of the statistical analysis of the data; Y-M.H. and K.L.E. designed the mouse trachea IV-TPM protocol and Y-M.H. performed in vivo imagings and helped in the data analysis; K.L.E., T.C., and S.B helped in the virus infection and mouse T cell preparations. T.C. performed the transwell assay. D.J.T. designed the influenza-infection model of mouse trachea. M.K. conceived, designed and directed the study. K.L. and M.K. wrote the manuscript with suggestions from all authors.

The authors have no conflicting financial interests.

Neutrophils are key players that help organs initiate and maintain immune reactions (10) and shape the overall immune response by signaling to DCs, monocytes, and T cells. Under most inflammatory conditions, neutrophils are the first cell type that crosses the blood vessel endothelium into the tissue, often preceding a subsequent wave of effector T cells (11, 12). Although neutrophil-mediated recruitment of T cells into infected sites has been documented in both bacterial and viral infections and in chronic inflammatory diseases (13–18), the molecular mechanisms that link neutrophil and T cell migration remain unknown.

## Results

### Reduced CD8$^+$ T cell response in the influenza infected trachea of the neutropenic mice

To investigate the role of neutrophil recruitment in shaping CD8$^+$ T cell responses during influenza infection, we first measured the kinetics of neutrophil and CD8$^+$ T cell responses in the trachea of C57BL/6 mice infected with influenza A virus. Infection of mice with $3 \times 10^4$ plaque-forming units (PFUs) of HKx31 influenza virus resulted in the rapid but transient infiltration of neutrophils to the trachea, with increases in cell number peaking at day 4, followed by the subsequent recruitment of CD8$^+$ T cells between days 6 and 8 (Fig. 1, A and B). Highly selective and near complete (> 95%) neutrophil depletion was then established using mAb 1A8 (anti-Ly6G) (fig. S1, A and B). Examination of trachea tissue at day 7 post-infection revealed that the depletion of neutrophils during infection elicited a significant delay in influenza virus clearance (Fig. 1C). This delay in virus clearance did not promote a more robust anti-viral CD8$^+$ T cell response (fig. S1, C and D); instead, neutrophil depletion following the primary infection of C57BL/6 mice with HKx31 reduced the total CD8$^+$ T cell response and significantly decreased the number of CD8$^+$ T cells specific for the influenza A virus nucleoprotein-derived epitope presented by H2-Db ($D^bNP_{366}$) (Fig. 1D).

Upon resolution, local tissue-resident memory T cells normally provide protection during lethal secondary virus challenge (19, 20). The number of memory T cells both in the lung and trachea, but not lymphoid memory T cells, was significantly lower when neutrophils were depleted during the primary infection (Fig. 1E). As shown previously (21), similar numbers of total $D^bNP_{366}$-specific CD8$^+$ T cells were recovered from draining lymph nodes of IgG- versus mAb 1A8-treated mice during the primary infection (fig. S1, C and D), suggesting that the absence of neutrophils reduced the magnitude of the influenza-specific CD8$^+$ T cell response as well as its memory without altering T cell priming and expansion.

The observed difference in CD8$^+$ T cell homing after neutrophil depletion was further examined by whole-mount immunostaining of CD8$^+$ T cells within the HKx31 infected trachea. CD8$^+$ T cells were strictly visible in the subepithelium, while many T cells remained in the interstitium and more distal to the epithelium after neutrophil depletion (Fig. 2A). To further examine the dynamics of influenza-specific CD8$^+$ T cells in the trachea, we transferred $2 \times 10^6$ splenocytes from a naive green fluorescent protein (GFP)-expressing OT-I T cell receptor (TCR) transgenic mouse (OT-$I^{GFP}$; the OT-I TCR recognizes a peptide fragment of chicken ovalbumin (OVA)), into the recipient mice one day prior to HKx31-OVA virus (22) inoculation. We then performed intravital two-photon microscopy (IV-TPM) on the surgically cannulated trachea (fig. S2). On day 7 post-infection, we found a large number of GFP-positive CD8$^+$ T cells actively migrating through out the trachea (Fig.

2B). As a substantial number of cells accumulated along the infected epithelium, the T cells became less motile, with a lower mean velocity and displacement (Fig. 2, B and C and movie S1). Furthermore, T cell migration appeared to be random, with confined motion for the imaging periods (movie S1). Similar to our observations using whole-mount immunostaining, fewer T cells were found to be localized within the vicinity of the epithelium of influenza-infected mouse trachea after neutrophil depletion (Fig. 2B and movie S2). Additionally, the movement of $CD8^+$ T cells occurred at a higher mean velocity and displacement in the parenchyma upon neutrophil depletion (Fig. 2C). This significant change in $CD8^+$ T cell speed and displacement after neutrophil depletion was observed in all examined mice and did not depend on the local T cell abundance. These results suggest that the relative motility of virus-specific $CD8^+$ T cells in the trachea is determined by their localization to the epithelium, which is governed by the presence of neutrophils during early infection.

## Neutrophil-derived chemokine induces $CD8^+$ T cell migration

Under inflammatory conditions, neutrophils release matrix metalloproteases (MMP-2 and -9), which are capable of remodeling the extracellular matrix (ECM) by cleaving type IV collagen present in the basement membrane (23, 24). Therefore, we used MMP-2/9 inhibitor I (25) to assess whether ECM modification by neutrophil-derived MMPs is an important part of $CD8^+$ T cell homing during influenza infection. Treatment of influenza-infected mice with the inhibitor did not have significant effects on T cell, suggesting that neutrophil-derived MMPs have a minimal impact on the initial T cell homing to influenza-infected trachea (fig. S3).

In addition to proteolytic enzymes, neutrophils release a variety of cytokines, which can lead to the amplification of many T cell functions during infection. The finding that the initial infiltration of neutrophils directly correlates with virus-specific $CD8^+$ T cell recruitment to the infected trachea suggests that neutrophils may be a major source of chemokines during influenza infection or may be mediators of chemoattractant release from infected cells. To examine chemokine production by murine neutrophils, we first screened 21 mouse chemokines and detected nine chemokines in neutrophil lysates prepared from both naïve and influenza-infected (day 4) mice (Fig. 3A). The activated $CD8^+$ T cells were found to express receptors that could recognize at least six of the nine detected chemokines (fig. S4 and ref. (26, 27)). Two known neutrophil chemokines, CXCL1 and CXCL2, were excluded from the analysis due to the lack of receptor expression on $CD8^+$ T cells (fig. S4). Among the six chemokines tested for $CD8^+$ T cell migration, only CXCL12 significantly induced cell migration *in vitro* (Fig. 3B), and this effect was completely abolished by the CXCR4 antagonist AMD3100 (Fig. 3C). The changes in $CD8^+$ T cell recruitment and location after neutrophil depletion *in vivo* were recapitulated by treating mice with AMD3100 (Fig. 3, D and E), suggesting that the $CD8^+$ T cell response during influenza infection is dependent on CXCL12 signals.

Although CXCL12 expression by non-hematopoietic cells in multiple tissues and its pleiotropic functions both in organ development and in the peripheral immune system are well established (28), relatively little is known regarding the CXCL12 that is released by

newly infiltrating immune cells during infections. To visualize the local expression of CXCL12 after influenza infection, we infected CXCL12-reporter mice ($CXCL12^{DsRed}$ knock-in mice that express DsRed under the endogenous *Cxcl12* promoter, ref. (29)) with HKx31 virus. Consistent with previous reports (29, 30), CXCL12 was primarily expressed by endothelial and perivascular stromal cells, as well as by epithelial cells of the naïve trachea (movie S3). Furthermore, the CXCL12 expression patterns in these non-motile cells were similar, irrespective of virus infection. On day 2 post-infection, we detected additional CXCL12+ cells that actively migrated throughout the interstitium of the trachea and more than 95% of these CXCL12+ motile cells were Ly6G-positive (Fig. 3F and movie S4). Thus, identifying CXCL12 reporter cells allowed us to observe that, among the innate immune cells that are recruited during early influenza infection, neutrophils are the main producers of local CXCL12 signals in the trachea. To further confirm that the neutrophil-derived, local CXCL12 signal is critical for $CD8^+$ T cell recruitment, we generated a granulocyte-specific CXCL12 conditional knock-out mouse (CXCL12-cKO) by crossing $CXCL12^{flox}$ + $Ela2^{Cre}$ mice (fig. S5, A and B). Deletion of CXCL12 in neutrophils resulted in a significant delay in $D^bNP_{366}$-specific $CD8^+$ T cell recruitment and disrupted localization in the trachea compared to the control CXCL12-floxed mice after influenza infection (Fig. 3G and fig. S6). Virus titers at the peak were identical in all strains of mice, though the CXCL12 deficient mice had slightly delayed virus clearance, similar to neutrophil depleted mice (Fig. 3H). This decrease in T cell response was likely due to the reduced total CXCL12 level in the trachea, as measured by total CXCL12 immunofluorescence intensity after day 7 of infection (Fig. 3I).

## Neutrophil leaves chemokine-containing trails

Although neutrophils produce a wide range of cytokines and chemokines, little is known about their release. Surprisingly, even high concentrations of inflammatory stimuli, such as tumor necrosis factor α (TNFα) (Fig. 4A and fig. S7) or fMLP, we failed to detect a significant release of soluble CXCL12 from neutrophils, whereas stimulation with PMA caused the dramatic secretion of CXCL12. To assess whether inflammatory signals that induce active neutrophil migration predispose neutrophils to release more CXCL12 and thus successfully induce $CD8^+$ T cell migration, we collected supernatant from actively migrating neutrophils and measured the CXCL12 level and its impact on $CD8^+$ T cell migration. Again, we could not detect a significant amount of CXCL12 in the supernatant, nor did it induce $CD8^+$ T cell chemokinesis (Fig. 4B). To test whether the minimum amount of CXCL12 released from migrating neutrophils could bind to glycosaminoglycan-coated surfaces and induce haptotactic $CD8^+$ T cell migration (31, 32), we incubated heparan sulfate (HS)-coated coverslips with the neutrophil supernatant and subsequently measured $CD8^+$ T cell migration. Even after prolonged incubation with the supernatant, the HS +ICAM-1-coated coverslip failed to induce $CD8^+$ T cell migration (Fig. 4B). To further test our hypothesis that migrating neutrophils release CXCL12 in a highly confined proximal area to guide only closely adjacent $CD8^+$ T cell chemotaxis in a chase-and-run fashion, we co-incubated neutrophils and $CD8^+$ T cells on ICAM-1-coated plates. fMLP was used to induce cell migration only in neutrophils (fig. S8) and the migration of each $CD8^+$ T cell was tracked beginning with its first physical encounter with a migrating neutrophil. The

spontaneous $CD8^+$ T cell migration was carried out in a random fashion, without any significant positive correlation with the neutrophil migration tracks (Fig. 4C).

To screen for potential $CD8^+$ T cell chemotactic signals that could be generated during neutrophil migration, we next turned our attention to neutrophil-experienced assay coverslips and measured cell migration on the neutrophil-experienced surface, after the migrating neutrophils were completely removed by extensive washing of the glass surface. To our surprise, the migration of activated $CD8^+$ T cells was most significantly enhanced in the absence of any additional exogenous chemotactic signals, whereas other cell types ($CD4^+$ T cells, neutrophils, and monocytes) showed no or minimally enhanced migration (Fig. 4D). The inhibition of CXCR4 with AMD3100 completely abolished this $CD8^+$ T cell migration, suggesting that the $CD8^+$ T cell migration on neutrophil-experienced coverslips depended on CXCL12 signals (Fig. 4E). First, we reasoned that a few damaged neutrophils had remained on the coverslip after washing and had released CXCL12 during the assay. We therefore used a fluorescently labeled Ly6G antibody to visualize any remaining neutrophils on the coverslip after our extensive washings. Unlike our prediction, we could not detect any remaining neutrophil cell bodies on the glass surface, but we did observe a substantial amount of membrane particles that were deposited on the coverslip (fig. S9). To determine whether the membrane particles were parts of damaged neutrophils that had been left behind during detachment or if the particles had been actively deposited along the membrane trail during migration by neutrophils, neutrophils labeled with FITC-conjugated Ly6G Ab were allowed to migrate on the coverslip. Live fluorescence imaging showed that the neutrophils formed long membrane tethers during migration and subsequently left behind membranous trails (Fig. 4F and movie S5). Scanning electron microscopy (SEM) of the migrating neutrophils further confirmed the ultrastructure of these neutrophil trails (Fig. 4G). Similar neutrophil trails were observed on ICAM-1-coated surfaces under both static and shear (1 $dyne/cm^2$) conditions (Fig. 4H). Moreover, the formation of neutrophil trails was inhibited by a specific LFA-1-blocking Ab on ICAM-1, and by a Mac-1-blocking Ab on fibronectin (FN)-coated surface (Fig. 4I), suggesting an important role for integrins in the formation of neutrophil trails.

In *Dictyostelium*, which responds to cAMP for chemotaxis, the enzyme that generates cAMP is highly enriched in the membrane vesicles that are deposited behind migrating cells (33). cAMP is released from these vesicles to prompt fellow cells to align and generate their head-to-tail streaming migration patterns. We hypothesized that similar membrane shedding and chemotactic signal compartmentalization exist for neutrophils during normal immune responses (34). To test this hypothesis, we characterized the chemokine composition of neutrophil-derived membrane trails. The mouse chemokine antibody array data showed that among the more than 50 cytokines/chemokines that were screened, only CXCL12 was preferentially enriched in the trails generated from the uropods of migrating neutrophils (Fig. 5A). We also detected abundant CXCL12 in many scattered vesicles inside the elongated neutrophil uropods, using a highly specific Ab against mouse CXCL12 (Fig. 5B and fig. S10). Immunohistologic examination of mouse neutrophils suggests that CXCL12 is stored within myeloperoxidase (primary granule)-, lactoferrin (secondary granule)-, and MMP9 (tertiary granule)-negative organelles, which may be secretory vesicles (fig. S11)

(35). To further determine whether the enhanced $CD8^+$ T cell migration on the neutrophil-experienced coverslip was directly mediated by CXCL12 derived from neutrophil trails, we used the granulocyte-specific CXCL12 conditional KO mouse (CXCL12-cKO). First, we allowed CXCL12-cKO neutrophils to migrate on an ICAM-1-coated glass surface in the presence of fMLP. After we confirmed the generation of neutrophil trails on the glass surface, the neutrophil cell bodies were removed, with minimal detachment of their trails. Subsequently, $CD8^+$ T cells were added, and their migration was analyzed. Unlike $CD8^+$ T cell migration on the WT neutrophil-preconditioned coverslip, T cell migration on the CXCL12-cKO neutrophil-experienced coverslip was not significantly increased (Fig. 5C).

Unlike neutrophils, which often show highly coordinated directional chemotaxis in tissues, T cells migrating in both lymphoid and non-lymphoid tissues have been observed to migrate by chemokine-mediated random or generalized Lévy walks (36, 37). The fact that the neutrophil trail did not directly induce the chemotaxis of adjacent $CD8^+$ T cells in a chase-andrun fashion (Fig. 4C) indicated that the trails might function as a slow-release CXCL12 depot or as a haptotactic CXCL12 signal that directly enhances $CD8^+$ T cell migration upon contact. To further dissect this, we performed a microchamber chemotaxis assay (Fig. 5D). Neutrophils were first placed in the left-side well (“neutrophil zone”) and were then allowed to migrate on an ICAM-1 or fibronectin-coated surface in the presence of fMLP, which permitted them to deposit trails in the “neutrophil zone”. After removing the neutrophils from the “neutrophil zone”, $CD8^+$ T cells were placed in the right-side well (“T cell zone”); the separation wall (500 μm in width) was then removed, and the T cells were followed by video microscopy. Within five to ten minutes after the onset of migration, the $CD8^+$ T cells in the “T cell zone” began to move toward the “neutrophil zone”, whereas the $CD8^+$ T cells that were placed next to the non-neutrophil- or CXCL12 cKO neutrophil-preconditioned “neutrophil zone” were unresponsive (Fig. 5D). These observations suggested that neutrophil trails indeed release a soluble factor that attracts $CD8^+$ T cells from a long distance (>500 μm).

## Neutrophil leaves CXCL12-containing trails in the tissues

Previously, we and others reported extreme uropod elongation during neutrophil extravasation *in vivo* (38–40). We observed that neutrophil uropods became elongated and left behind membrane trails during extravasation and interstitial migration in influenza-infected trachea (Fig. 6, A to C and movie S6 to S8). Indeed, many neutrophils appeared to be crawling in directional patterns that closely followed the local collagen fibers based on second-harmonic generation (SHG) signals. Using mice expressing mRFP tagged CXCL12 (41), we further confirmed that CXCL12-containing neutrophil trails were preferentially deposited along the SHG fibers *in vivo* (Fig. 6D, fig. S12, and movie S9). Importantly, many $CD8^+$ T cells migrated in close contact with the local collagen structures (42), making serial contacts with the neutrophil trails (Fig. 6E and movie S10). The frequency of the direct contact between neutrophil trails and $CD8^+$ T cells during migration was significantly decreased in the presence of AMD3100 (Fig. 6F), suggesting that the interaction is dependent on CXCL12 signals.

To determine how long these neutrophil trails remain in the tissue, we first treated influenza-infected trachea with collagenase and removed all intact cells by slow speed centrifugation (fig. S13A). The trails deposited in the tissue were then measured by Western blot analysis of Ly6G signals in the digested trachea. The result showed that Ly6G-containing trails were persistent in the infected trachea during the infection (Fig. 7A). The prolonged retention of CXCL12-containing Ly6G+ trails was further confirmed by isolating the micro-size trail particles using ultracentrifugation (43, 44) and by immunostaining (fig. S13, B and C). These data demonstrated that the signature of deposited neutrophil trails (Ly6G) remained in the tissue until the host cleared an infection and led us to hypothesize that the trails could provide prolonged local CXCL12 signals, even after the early marginated neutrophil pools were cleared from the infected trachea (Fig. 1B). To test this hypothesis, we measured the CXCL12 levels within the trachea. Whole-mount immunostainings of previously fixed and permeabilized mouse trachea cross-sections revealed a lining of CXCL12 staining that was exclusively associated with the epithelium (D0 in Fig. 7D), which suggested that the main source of CXCL12 production in the non-infected trachea is the epithelium (30). Upon influenza infection, the overall intensity of the CXCL12 signal was significantly increased in the WT trachea, but not in the CXCL12 cKO mice (Fig. 7B), and data integration from multiple trachea sections revealed that the increase in CXCL12 signal during infection mainly occurred in the interstitial area (Fig. 7C). We calculated the colocalization coefficient to estimate how well the detected CXCL12 signals complied with the distribution of CXCL12-producing cells ($CXCL12^{DsRed}$) within the trachea during infection and found that the CXCL12 and $CXCL12^{DsRed}$ signals were closely localized within the naïve trachea (D0 in Fig. 7, D and E), suggesting that the CXCL12 produced by epithelial cells remains in close proximity to the epithelium. However, the colocalization coefficient was dramatically decreased during influenza infection, though the total CXCL12 intensity increased (D4 and D8 in Fig. 7, D and E). These results indicate that either epithelial cell-derived CXCL12 diffuses widely in a tissue or that newly infiltrated migratory cells release and deposit CXCL12 in the interstitium. Importantly, the depletion of neutrophils during infection prevented a decrease in the colocalization coefficient and abolished the increase in total CXCL12 intensity in the trachea (Fig. 7F), suggesting that newly recruited neutrophils during influenza infection are a main source of CXCL12.

## Discussion

The recruitment of leukocyte subtypes into peripheral tissues occurs in cascades, with the movement of one cell type following the remodeling of the local tissue environment, thereby inducing and regulating the recruitment of the next wave of immune cells (45). Given the complexity and multifaceted pathophysiology of influenza infection and the high degree of redundancy of the homing receptors on the T cell surface, we hypothesized that specific combinations of local tissue milieus created by early innate responses regulate chemoattractant signals to control the recruitment of effector T cells to the infected sites. Indeed, influenza infection causes rapid expression of high levels of inflammatory chemokines, including CCL2, CCL3, CCL5, and CXCL10 (46). Furthermore, the newly activated effector CD8 T cells released from lymphoid organs express diverse inflammatory chemokine receptors, such as CCR2, CCR5, and CXCR3 (47). Therefore, it is possible that

multiple chemokines cooperate temporally and spatially to finely control the movement of T cells and to prioritize their responses to the different chemokines present in the inflamed tissues. Alternatively, a hierarchy of chemokine response may exist, in which certain chemokines initially dominate other local chemokine signals; this signal is then desensitized, and the T cells follow a new gradient of local chemokines in a sequential manner. In both cases, inhibition of any single chemokine would cause a profound effect on T cell trafficking, as we have seen with CXCL12 inhibition. The data presented here demonstrate that migrating neutrophils leave behind chemoattractant-containing trails, resulting in the local accumulation of neutrophil-derived chemoattractant signals in inflamed tissues. As chemokines are small, diffusible molecules, perhaps these trails serve to package the chemoattractant so that it can be preserved and survive severe mechanical perturbation during inflammation (48), lest it be present only transiently on cell surfaces and tissue matrix or immediately diffuse away from the site.

The fact that $CD8^+$ T cell recruitment and virus clearance were both affected in the CXCL12 cKO mice in spite of the presence of epithelial cell derived CXCL12 argues that this is not the relevant source of the chemokine during the infection. Based on our data, we concluded that CXCL12 derived from the epithelial cells remained close to the epithelium, while CXCL12 derived from neutrophils was the main source of CXCL12 in the tissue interstitium during infection. The fact that CXCL12 expressed by the epithelial cells remains in close proximity to the epithelium and does not diffuse widely to the interstitium is an interesting topic. This may be due at least in part to high expression of CXCR7 (another high affinity receptor for CXCL12) in epithelial cells (49). CXCR7 acts as a scavenger receptor for CXCL12, sequestering and reducing the level of CXCL12 at tissues to maintain a chemotactic gradient (50, 51).

Unlike in our *in vitro* study, neutrophil trails were sparsely distributed and rather rarely shown in the *in vivo* imaging. We previously showed that microparticles generated from neutrophil trails had multiple spherical shapes ranging from 100 to 500 nm in diameter (38). Currently it is not possible to detect small microparticles (<0.5 μm) *in vivo* due to the resolution limit of multi photon intravital microscopy. Therefore it is tempting to speculate that we only show big neutrophil microparticles (bigger than 500 nm in diameter) in our in vivo images, while small, undetected particles still can guide CD8 T cell migration.

Neutrophils can express and/or produce numerous cytokines (including IFN-γ) that can alter local $CD8^+$ T cell activation. Indeed, the virus-specific $CD8^+$ T cells in the influenza-infected airway displayed impaired cytokine production and cytotoxic effector function in the absence of neutrophils without significant changes in influenza virus-specific antigen presentation or $CD8^+$ T cell priming in the secondary lymphoid organs (21). Together with our results, these data strongly suggest that the absence of neutrophils not only impairs the establishment of a sustained $CD8^+$ T cell population at the site of infection through altered $CD8^+$ T cell traffic and localization, but it also greatly diminished the effector function of the remaining $CD8^+$ T cells. Currently, however, casual relation between neutrophil-mediated $CD8^+$ T cells migration and activation of local $CD8^+$ T cell effector functions is unknown.

## Materials and Methods

### Antibodies and reagents

Recombinant mouse proteins (ICAM-1, CXCL12, CCL2, CCL6, CCL12, CCL22, CCL27, TNFα) and carboxyfluorescein (CFS)-, phycoerythrin (PE), or allophycoerythrin (APC)-conjugated anti-CXCL12 (79018), APC-conjugated anti-CCR1 (643854), APC-conjugated anti-CCR2 (475301), APC-conjugated anti-CXCR2 (242216), anti-myeloperoxidase (392105) antibodies were purchased from R&D systems. PE-conjugated anti-CXCR4 (2B11) and Alexa Fluor 647-conjugated anti-CD8 (53–6.7) were purchased from eBioscience. Fluorescein isothiocyanate (FITC)-conjugated, APC-conjugated, or unconjugated anti-Ly6G (1A8), FITC- or Alexa Fluor 647-conjugated anti-Gr1 (RB6-8C5), PE-conjugated anti-CCL2 (2H5), anti-CD11a integrin (M17/4), anti-CD11b integrin (M1/70), anti-β1 integrin (HMB1-1), rat IgG2a, and rat IgG2b antibodies were purchased from Biolegend. Anti-Ly6G antibody (1A8) for neutrophil depletion and rat IgG2a control antibody (2A3) were purchased from BioXcell. Anti-fibronectin (96–23750) and anti-CXCR1 antibody (ab10400) were from Abcam. Alexa Fluor 488-conjugated anti-F4/80 (BM8) and Alexa Fluor 647-conjugated anti-goat IgG antibodies were purchased from Invitrogen. Anti-CD3e (145-2C11), anti-CD28 (37.51) and FITC-conjugated anti-CD45 (553772) antibodies were purchased from BD Bioscience. Anti-type IV collagen antibody (1340-01) was purchased from Southern Biotechnology. The antibody to influenza A virus nucleoprotein (NP) conjugated with FITC was purchased from ViroStat. Anti-CXCL12 (C-19), anti-matrix metalloproteinase 9 (sc-6841) and anti-lactoferrin (sc-25622) antibodies were from Santa Cruz Biotechnology. Horseradish peroxidase-conjugated anti-mouse IgG or anti-rat IgG, and Cy3-conjugated anti-goat IgG antibodies were from Jackson ImmunoResearch. Heparan sulfate, DAPI, Texas red-conjugated dextran, fMLP, and saponin were purchased from Sigma Aldrich. AMD3100 was purchased from Tocris. MMP-2/9 inhibitor I was from Calbiochem (25). A chemiluminescent reagent (Supersignal West Pico) was from Thermo Scientific.

### Mice

C57BL/6, *Tyr*$^{c\text{-}2J/c\text{-}2J}$ (B6-Albino), and *CXCL12*$^{flox/flox}$ mice were purchased from the Jackson Laboratory. CXCL12$^{DsRed}$ mouse was the gift from Dr. Sean Morrison (29). OT-I TCR transgenic mouse was crossed with *C57BL/6-Tg(CAG-EGFP)1Osb/J* (Jackson Laboratory) for EGFP-expressing OT-1 strain (OT-1$^{GFP}$). *CXCL12*$^{flox/flox}$ was crossed with elastase2 (*Ela*)$^{Cre/+}$ for granulocyte-specific knock-out of CXCL12 and *CXCL12*$^{flox/flox}$*Ela*$^{Cre/+}$ mice were used for experiments with their littermates *CXCL12*$^{flox/flox}$*Ela*$^{+/+}$ or *Ela*$^{Cre/+}$ as a control group. Genotyping for each strain was performed according to the corresponding reference (29). All mice were maintained in a pathogen-free environment of the University of Rochester animal facility and the animal experiments were approved by the University Committee on Animal Resources at the University of Rochester (Rochester, NY, USA).

### Influenza virus and neutrophil depletion

Eight to twelve-week-old male mice were anesthetized using Avertin (2,2,2-tribromoethanol) and intranasally inoculated with 30 μl of influenza A virus suspension

(HKx31, $3 \times 10^4$ PFU and HKx31-OVA, $3 \times 10^{3.25}$ EID50). For neutrophil depletion, 500 μg of Ly6G antibody (1A8) was intraperitoneally injected to a mouse at a day before infection and, day +1, +3, and +5 post-infection and isotype control IgG (rat IgG2a) was injected to a control group. For $CD8^+$ T cell imaging *in vivo*, splenocytes (2 million) from OT-$1^{GFP}$ mouse were injected to a recipient mouse via tail vein 24 hr before infection with HKx-31-OVA virus.

### Viral nucleoprotein mRNA levels in trachea

Total RNA from trachea was prepared using RNeasy kit (Qiagen) and the first-strand cDNA was synthesized using M-MLV reverse transcriptase (Promega) and oligo-$(dT)_{18}$. Quantitative RT-PCR was performed using SYBR green reagent (BioRad) and following primers; viral nucleoprotein gene, forward 5'-TTTTCTAGCACGGTCTGCACTCATATTG-3' reverse 5'-CTTGGCTGTTTTGAAGCAGTCTGAAAG-3', β-actin, forward 5'-GTCCCTCACCCTCCCAAAG-3' reverse 5'-GCTGCCTCAACACCTCAACC-3'. The levels of viral nucleoprotein mRNA were normalized by those of the actin mRNA.

### Leukocytes preparation

Neutrophils were freshly prepared from mouse bone marrow using EasySep Neutrophil enrichment kit (STEMCELL technology). $CD4^+$ and $CD8^+$ T lymphocytes from spleen and lymph node were isolated using a negative selection method and activated by culturing them on a CD3 (10 μg/ml) antibody-coated dish in the presence of CD28 (2 μg/ml) and 10 unit/ml IL-2. F4/80 positive mouse monocytes were isolated from blood using FACS sorting.

### *In vitro* migration

Cell migration chambers (Millicell EZ slide 8 well glass from Millipore or Delta T dish from Bioptech) were prepared by coating their glass bottom with 10 μg/ml recombinant mouse ICAM-1 or mouse fibronectin in PBS with or without indicated chemokines. For *in vitro* live cell imaging, leukocytes were placed in L15 medium (Invitrogen) in the chamber at 37°C and video microscopy was conducted using TE2000-U microscope (Nikon). Images were acquired using ×10, ×20, or ×60 magnification objective with the appropriate filters. Migration analysis and image processes were performed using NIS (Nikon) or Volocity software (PerkinElmer). For integrin blocking, neutrophils were pre-incubated with the indicated blocking antibodies (10 μg/ml) for 10 min and allowed to crawl in the presence of the same antibody. For migration under shear, fMLP-stimulated neutrophils stained with FITC-Ly6G were allowed to crawl in ICAM-1 coated μ-Slide I 0.8 Luer flow chamber (Ibidi) and flow was created by a syringe pump. For chemotaxis assay, the chamber (Millicell EZ slide 4 well glass, Millipore) was coated with 5 μg/ml fibronectin and 0.25 μg/ml ICAM-1 overnight. Next day, the chamber was washed and the culture insert from a wound healing dish (30 μ-Dish culture insert, Ibidi) was placed. fMLP-stimulated neutrophils were allowed to crawl in the left well and washed after 20 min. $CD8^+$ T cells were then added to the right well and allowed to adhere for 10 min. Then, the insert was removed and T cell migration was tracked for 1 hr.

For transwell assay, $1 \times 10^4$/100 μl of T cells were added in 5-μm pore-size, polycarbonate 24-well tissue culture inserts (Costar, Cambridge, MA), while 600 μl of medium with or without a chemoattractant (CXCL12 or fMLP) was added to the lower well. After 3 hours, counting beads were added to the lower chamber and collected for flow cytometric analysis. Cell number was determined relative to the number of beads collected. All points were performed in triplicate for multiple mice ($n \geq 3$).

### Immunofluorescence microscopy

For immunofluorescence microscopy of trachea, 10-μm thickness frozen trachea sections were prepared and stained with the indicated antibodies. Superblock (Thermo Scientific) was used as a blocker. Quantitative analysis of fluorescent signals was performed using NIS (Nikon) or Autoquant X software (MediaCybernetics). For immunofluorescence microscopy of neutrophils, cells were fixed with 2% paraformaldehyde and stained with the indicated antibodies in the presence of 0.025% saponin.

### Flow cytometry

Trachea was digested with 1 mg/ml collagenase II (Gibco) for 1 hr at 37 °C with frequent agitations and the digests were filtered through 70-μm strainer (BD Falcon). Single cell populations from lymph nodes, spleen, or lung were obtained by squeezing the tissue through 40-μm strainer followed by lysis of red blood cells. The isolated cells were stained with the indicated antibodies or APC-conjugated NP tetramer (NIH tetramer facility) and analyzed with FACS Caliber (BD biosciences). For intracellular staining, 0.1% Tween 20 was included during the staining and washing.

### Intravital two-photon microscopy (IV-TPM)

The mouse was anesthetized by intraperitoneally injecting pentobarbital sodium-salt (65 mg/kg). The trachea was exteriorized and a small cut on the frontal wall to insert an 18G blunt-end cannula. To discern the border of epithelium in the luminal side, the cannula was painted in red color. Ly6G-FITC antibody (20 μg) and Texas red-conjugated dextran (20 mg/kg) were injected via femoral vein to stain neutrophils and blood vessel, respectively. The mouse was subsequently placed on a custom-designed platform for imaging (fig. S2). For IV-TPM of the mouse ear, $5 \times 10^4$ neutrophils with or without $5 \times 10^4$ $CD8^+$ T cells in 5 μl PBS were intradermally injected to *Tyr*$^{c\text{-}2J/c\text{-}2J}$ (B6-Albino) mouse 3 hr prior to imaging. For the control, cells ($1 \times 10^7$ cells/ml PBS) were treated with AMD3100 (25 μM) for 30 min before intradermal injection. To visualize $CD8^+$ T cells and neutrophils simultaneously, $CD8^+$ T cells were prepared from *C57BL/6-Tg(CAG-EGFP)1Osb/J* mouse and WT neutrophils were stained with red dye (CMTPX, Life Technologies). The anesthetized mouse was laid in a lateral recumbent position on a custom-designed platform to expose the ventral side of the ear pinna for imaging. Further anesthesia was maintained with isoflurane for restraint and to avoid psychological stress and pain on the animal during imaging. The mouse was imaged with FV1000-AOM multiphoton system using ×25 NA1.05 objective (Olympus). During imaging, both mouse body and the objective were maintained at 37°C. For whole mount tissue imaging, the trachea was fixed with paraformaldehyde, blocked and permeabilized with Superblock (Thermo Scientific) containing 0.1% Tween 20. CXCL12

was stained with 0.5 μg/ml anti-CXCL12 antibody (C-19; Santa Cruz biotechnology) for overnight at 4 °C. Imaging data were processed using Volocity (PerkinElmer) and Image J.

### Scanning electron microscopy

Neutrophils migrating on ICAM-1 coated glass were fixed with 2.5% glutaraldehyde and processed further for scanning electron microscopy in the Electron Microscope Research Core at the University of Rochester.

### Chemokine microarray

To collect neutrophil trails, neutrophils were allowed to migrate on ICAM-1 coated glass in the presence of 2 μM fMLP for one hour. Then, neutrophil cell bodies were removed and the remaining trails were lysed by adding 1% Triton-containing PBS supplemented with 1 mM EDTA and protease inhibitor cocktail (Roche). The whole cell neutrophil lysate was prepared in the same lysis buffer. The amount and quality of extracted proteins were checked by Nanodrop (Thermo Scientific) and silver staining following gel electrophoresis of proteins. The microarray was carried out using Proteome Profiler Mouse chemokine and cytokine array (R&D systems) according to the manufacturer's instruction. This antibody array detects CCL11, CCL12, CCL2, CCL21, CCL22, CCL27, CCL28, CCL3/4, CCL5, CCL6, CCL8, CCL9, Chemerin, Complement component C5, CX3CL1, CXCL1, CXCL10, CXCL11, CXCL12, CXCL13, CXCL16, CXCL2, LIX, CXCL9, and IL-16.

### Western blot analysis of trails

The trachea was digested with collagenase and intact cells were removed by centrifugation at 1000g for 30 min before Western blot analysis. To directly collect neutrophil trails from the trachea, the supernatant was further centrifuged at 18,000g for 1 hr. For Western blotting, the membrane was blocked with a blocker (3% BSA, 0.1% Tween 20 in PBS) for 30 min after proteins were transfer from a gel and incubated with 0.5 μg/ml of 1A8 antibody for 1 hr at room temperature. Then, the membrane was incubated with horseradish peroxidase-conjugated anti-rat IgG antibody (0.4 μg/ml) for 1 hr and the protein was detected using a chemiluminescent reagent. The intensity of Ly6G protein band was normalized by that of fibronectin.

### Enzyme-linked immunosorbent assay (ELISA)

Neutrophils ($5 \times 10^6$ cells) were stimulated by incubating them in L15 medium containing indicated concentrations of TNFα or PMA at 37°C for 1 hr. The amount of CXCL12 in the supernatants was measured using Quantikine ELISA (R&D systems).

## Supplementary Material

Refer to Web version on PubMed Central for supplementary material.

## Acknowledgments

We thank Alison Gaylo, Yuexin Xu, Brandon Walling, Jennifer Wong, Nathan Laniewski, Hongmei Yang, and Urmila Sivagnanalingam for their technical assistance and comments on manuscript, and thank S. Morrison for $CXCL12^{DsRed}$ mouse.

This project was financially supported through grants from the National Institute of Health (HL087088 to M.K. and AI102851 to M.K. & D.J.T., and HHSN272201400005C to D.J.T.), WCU Neurocytomics Program Grant to M.K., and the American Heart Association (11SDG7520018 to Y-M.H.).

## References

1. Griffith JW, Sokol CL, Luster AD. Chemokines and chemokine receptors: positioning cells for host defense and immunity. Annu Rev Immunol. 2014; 32:659–702. [PubMed: 24655300]
2. Agace WW. Tissue-tropic effector T cells: generation and targeting opportunities. Nature reviews. 2006; 6:682–692.
3. Ward SG, Marelli-Berg FM. Mechanisms of chemokine and antigen-dependent T-lymphocyte navigation. The Biochemical journal. 2009; 418:13–27. [PubMed: 19159344]
4. Schneider IC, Haugh JM. Mechanisms of gradient sensing and chemotaxis: conserved pathways, diverse regulation. Cell Cycle. 2006; 5:1130–1134. [PubMed: 16760661]
5. Scapini P, et al. The neutrophil as a cellular source of chemokines. Immunological reviews. 2000; 177:195–203. [PubMed: 11138776]
6. Luster AD. The role of chemokines in linking innate and adaptive immunity. Curr Opin Immunol. 2002; 14:129–135. [PubMed: 11790543]
7. Groom JR, et al. CXCR3 chemokine receptor-ligand interactions in the lymph node optimize CD4+ T helper 1 cell differentiation. Immunity. 2012; 37:1091–1103. [PubMed: 23123063]
8. Luster AD, Alon R, von Andrian UH. Immune cell migration in inflammation: present and future therapeutic targets. Nature immunology. 2005; 6:1182–1190. [PubMed: 16369557]
9. Galli SJ, Borregaard N, Wynn TA. Phenotypic and functional plasticity of cells of innate immunity: macrophages, mast cells and neutrophils. Nature immunology. 2011; 12:1035–1044. [PubMed: 22012443]
10. Nathan C. Neutrophils and immunity: challenges and opportunities. Nature reviews. 2006; 6:173–182.
11. Mantovani A, Cassatella MA, Costantini C, Jaillon S. Neutrophils in the activation and regulation of innate and adaptive immunity. Nature reviews. 2011; 11:519–531.
12. Summers C, et al. Neutrophil kinetics in health and disease. Trends in immunology. 2010; 31:318–324. [PubMed: 20620114]
13. Borregaard N, Sorensen OE, Theilgaard-Monch K. Neutrophil granules: a library of innate immunity proteins. Trends in immunology. 2007; 28:340–345. [PubMed: 17627888]
14. Olson TS, Ley K. Chemokines and chemokine receptors in leukocyte trafficking. Am J Physiol Regul Integr Comp Physiol. 2002; 283:R7–R28. [PubMed: 12069927]
15. Pelletier M, et al. Evidence for a cross-talk between human neutrophils and Th17 cells. Blood. 2010; 115:335–343. [PubMed: 19890092]
16. Grabie N, et al. Neutrophils sustain pathogenic CD8+ T cell responses in the heart. Am J Pathol. 2003; 163:2413–2420. [PubMed: 14633613]
17. de Oca RM, et al. Polymorphonuclear neutrophils are necessary for the recruitment of CD8(+) T cells in the liver in a pregnant mouse model of Chlamydophila abortus (Chlamydia psittaci serotype 1) infection. Infect Immun. 2000; 68:1746–1751. [PubMed: 10679002]
18. Engeman T, Gorbachev AV, Kish DD, Fairchild RL. The intensity of neutrophil infiltration controls the number of antigen-primed CD8 T cells recruited into cutaneous antigen challenge sites. Journal of leukocyte biology. 2004; 76:941–949. [PubMed: 15328335]
19. Ray SJ, et al. The collagen binding alpha1beta1 integrin VLA-1 regulates CD8 T cellmediated immune protection against heterologous influenza infection. Immunity. 2004; 20:167–179. [PubMed: 14975239]
20. Gebhardt T, et al. Memory T cells in nonlymphoid tissue that provide enhanced local immunity during infection with herpes simplex virus. Nature immunology. 2009; 10:524–530. [PubMed: 19305395]
21. Tate MD, Brooks AG, Reading PC, Mintern JD. Neutrophils sustain effective CD8(+) T-cell responses in the respiratory tract following influenza infection. Immunol Cell Biol. 2012; 90:197–205. [PubMed: 21483446]

22. Thomas PG, et al. An unexpected antibody response to an engineered influenza virus modifies CD8+ T cell responses. Proceedings of the National Academy of Sciences of the United States of America. 2006; 103:2764–2769. [PubMed: 16473934]
23. Chakrabarti S, Patel KD. Matrix metalloproteinase-2 (MMP-2) and MMP-9 in pulmonary pathology. Exp Lung Res. 2005; 31:599–621. [PubMed: 16019990]
24. Bradley LM, Douglass MF, Chatterjee D, Akira S, Baaten BJ. Matrix metalloprotease 9 mediates neutrophil migration into the airways in response to influenza virus-induced toll-like receptor signaling. PLoS Pathog. 2012; 8:e1002641. [PubMed: 22496659]
25. Tamura Y, et al. Highly selective and orally active inhibitors of type IV collagenase (MMP-9 and MMP-2): N-sulfonylamino acid derivatives. J Med Chem. 1998; 41:640–649. [PubMed: 9484512]
26. Gehad A, et al. Differing requirements for CCR4, E-selectin, and alpha4beta1 for the migration of memory CD4 and activated T cells to dermal inflammation. J Immunol. 2012; 189:337–346. [PubMed: 22664869]
27. Hudak S, et al. Immune surveillance and effector functions of CCR10(+) skin homing T cells. J Immunol. 2002; 169:1189–1196. [PubMed: 12133939]
28. Kucia M, et al. CXCR4-SDF-1 signalling, locomotion, chemotaxis and adhesion. J Mol Histol. 2004; 35:233–245. [PubMed: 15339043]
29. Ding L, Morrison SJ. Haematopoietic stem cells and early lymphoid progenitors occupy distinct bone marrow niches. Nature. 2013; 495:231–235. [PubMed: 23434755]
30. Gomperts BN, et al. Circulating progenitor epithelial cells traffic via CXCR4/CXCL12 in response to airway injury. J Immunol. 2006; 176:1916–1927. [PubMed: 16424223]
31. Campanella GS, et al. Oligomerization of CXCL10 is necessary for endothelial cell presentation and in vivo activity. J Immunol. 2006; 177:6991–6998. [PubMed: 17082614]
32. Weber M, et al. Interstitial dendritic cell guidance by haptotactic chemokine gradients. Science. 2013; 339:328–332. [PubMed: 23329049]
33. Kriebel PW, Barr VA, Rericha EC, Zhang G, Parent CA. Collective cell migration requires vesicular trafficking for chemoattractant delivery at the trailing edge. The Journal of cell biology. 2008; 183:949–961. [PubMed: 19047467]
34. Pruenster M, et al. The Duffy antigen receptor for chemokines transports chemokines and supports their promigratory activity. Nature immunology. 2009; 10:101–108. [PubMed: 19060902]
35. Soehnlein O, Zernecke A, Weber C. Neutrophils launch monocyte extravasation by release of granule proteins. Thromb Haemost. 2009; 102:198–205. [PubMed: 19652869]
36. Mueller SN. Effector T-cell responses in non-lymphoid tissues: insights from in vivo imaging. Immunol Cell Biol. 2013; 91:290–296. [PubMed: 23295362]
37. Harris TH, et al. Generalized Levy walks and the role of chemokines in migration of effector CD8+ T cells. Nature. 2012; 486:545–548. [PubMed: 22722867]
38. Hyun YM, et al. Uropod elongation is a common final step in leukocyte extravasation through inflamed vessels. The Journal of experimental medicine. 2012; 209:1349–1362. [PubMed: 22711877]
39. Sperandio M, et al. P-selectin glycoprotein ligand-1 mediates L-selectin-dependent leukocyte rolling in venules. J. Exp. Med. 2003; 197:1355–1363. [PubMed: 12756271]
40. Peters NC, et al. In vivo imaging reveals an essential role for neutrophils in leishmaniasis transmitted by sand flies. Science. 2008; 321:970–974. [PubMed: 18703742]
41. Mithal DS, Ren D, Miller RJ. CXCR4 signaling regulates radial glial morphology and cell fate during embryonic spinal cord development. Glia. 2013; 61:1288–1305. [PubMed: 23828719]
42. Overstreet MG, et al. Inflammation-induced interstitial migration of effector CD4(+) T cells is dependent on integrin alphaV. Nature immunology. 2013; 14:949–958. [PubMed: 23933892]
43. Dalli J, et al. Annexin 1 mediates the rapid anti-inflammatory effects of neutrophil-derived microparticles. Blood. 2008; 112:2512–2519. [PubMed: 18594025]
44. Pluskota E, et al. Expression, activation, and function of integrin alphaMbeta2 (Mac-1) on neutrophil-derived microparticles. Blood. 2008; 112:2327–2335. [PubMed: 18509085]
45. Sadik CD, Luster AD. Lipid-cytokine-chemokine cascades orchestrate leukocyte recruitment in inflammation. Journal of leukocyte biology. 2012; 91:207–215. [PubMed: 22058421]

46. Damjanovic D, Small CL, Jeyanathan M, McCormick S, Xing Z. Immunopathology in influenza virus infection: uncoupling the friend from foe. Clin Immunol. 2012; 144:57–69. [PubMed: 22673491]

47. Bromley SK, Mempel TR, Luster AD. Orchestrating the orchestrators: chemokines in control of T cell traffic. Nature immunology. 2008; 9:970–980. [PubMed: 18711434]

48. Majumdar R, Sixt M, Parent CA. New paradigms in the establishment and maintenance of gradients during directed cell migration. Current opinion in cell biology. 2014; 30:33–40. [PubMed: 24959970]

49. Balabanian K, et al. The chemokine SDF-1/CXCL12 binds to and signals through the orphan receptor RDC1 in T lymphocytes. The Journal of biological chemistry. 2005; 280:35760–35766. [PubMed: 16107333]

50. Boldajipour B, et al. Control of chemokine-guided cell migration by ligand sequestration. Cell. 2008; 132:463–473. [PubMed: 18267076]

51. Dambly-Chaudiere C, Cubedo N, Ghysen A. Control of cell migration in the development of the posterior lateral line: antagonistic interactions between the chemokine receptors CXCR4 and CXCR7/RDC1. BMC Dev Biol. 2007; 7:23. [PubMed: 17394634]

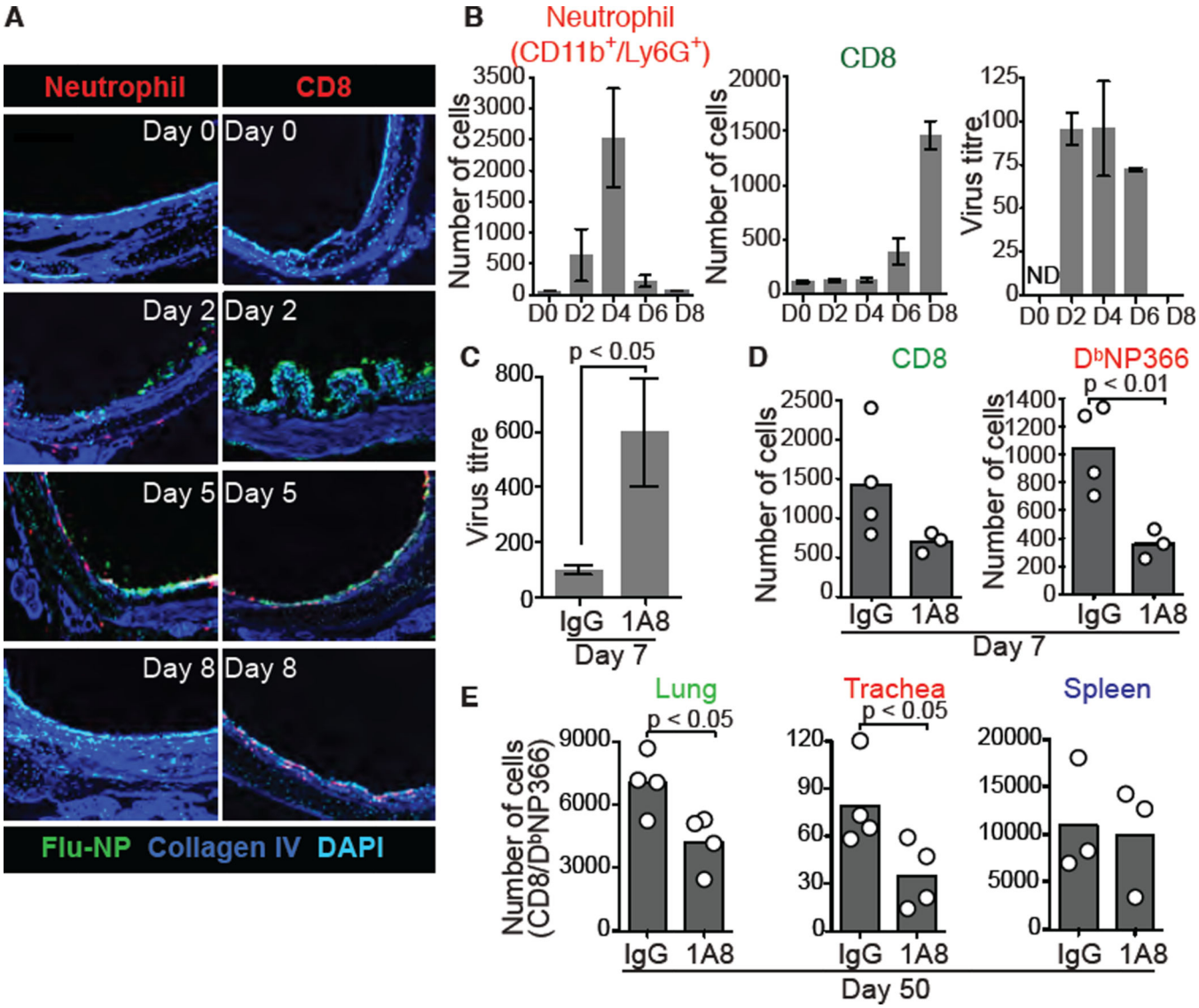


**Fig. 1. Reduced CD8$^+$ T cell response in the neutropenic mice**

(**A**) Immunofluorescence images of trachea sections from influenza virus-infected mice at the indicated days of post-infection. Red, neutrophils or CD8$^+$ T cells; green, viral nucleoprotein (NP); blue, collagen IV; cyan, nuclear staining with DAPI. Each panel showed one representative image from three repetitive experiments. Scale bar, 200 μm. (**B**) Flow cytometry analysis of neutrophils (left) and CD8$^+$ T lymphocytes (middle) in the trachea after influenza infection (mean ± SEM, $N \geq 3$ per group). Viral NP mRNA levels (right) normalized by cellular actin mRNA (%) in the trachea using qRT-PCR (at day 2 post-infection, mean ± SEM, $N = 3$ per group). ND, not detected. (**C**) Neutrophils were depleted by intraperitoneal injection of Ly6G antibody (1A8) at day −1, +1, +3, and +5 post-infection and viral loads were measured at day 7 (% of isotype control IgG-treated group (IgG), mean ± SEM, $N \geq 6$ per group). (**D**) Total or virus ($D^bNP_{366}$)-specific CD8$^+$ T cell numbers were counted from 1A8- or IgG-injected mice using flow cytometry at day 7 after infection. (**E**) Numbers of virus-specific memory CD8$^+$ T cells in the indicated tissues of mice with or

without neutrophil depletion were measured at day 50 post-infection. (**D** and **E**) points indicate data from individual mice. Statistical differences in (**C, D,** and **E**) were assessed using Student's t test.

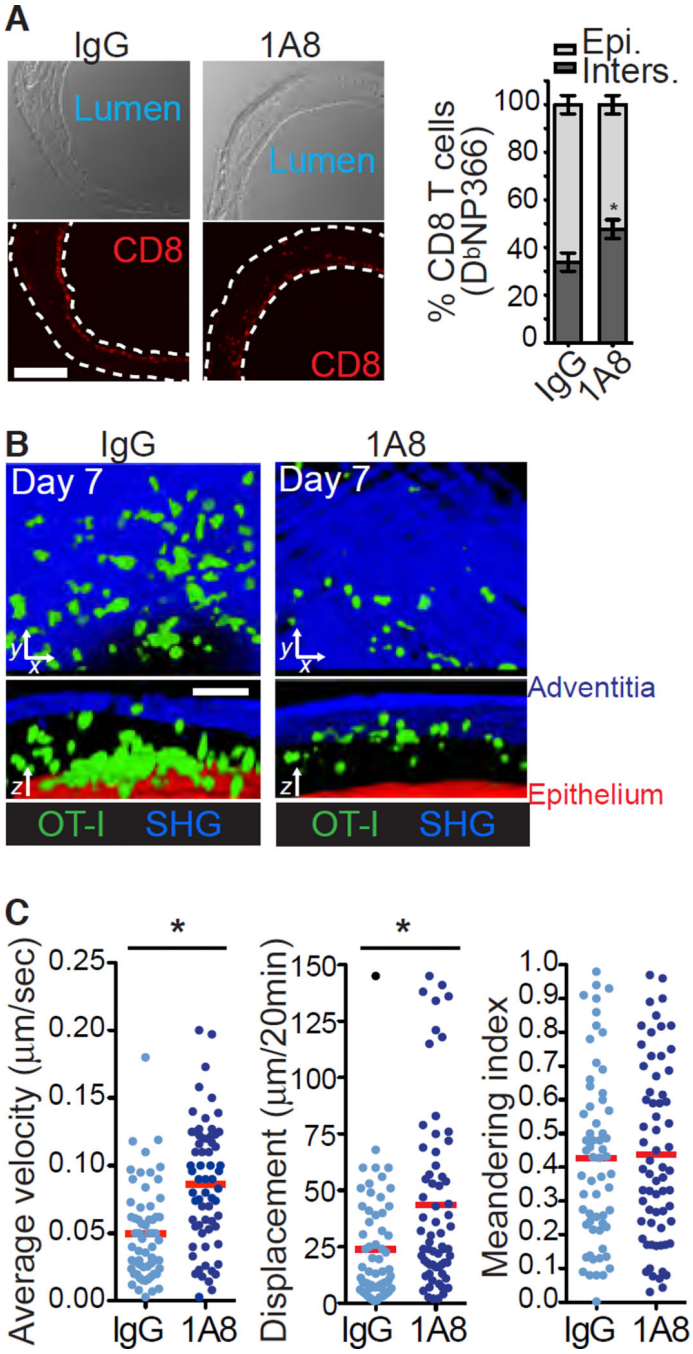


**Fig. 2. Location and migration of CD8$^+$ T cells in the neutropenic mice**

(**A**) Immunofluorescence images of the trachea sections from virus-infected mice with or without neutrophil depletion. Top, bright field; bottom, CD8$^+$ T cells (red). The dotted line indicates tracheal tissue borders. Graph, the ratio (% total) of the numbers of CD8$^+$ T cells in the epithelium or the interstitium ($N \geq 3$ sections from a mouse, $N \geq 3$ mice per group). *$P < 0.05$ compared with IgG. Epi., epithelium; Inters., interstitium. Scale bar, 200 µm. (**B**) *xy*-plane (top) and *z*-stacks (bottom) from a representative IV-TPM of OT-I$^{GFP}$ CD8$^+$ T cells in HKx31-OVA virus-infected trachea at day 7 post-infection with/without neutrophil

depletion. OVA-specific $CD8^+$ T cells (green), adventitia (blue) and the tracheal lumen (red) were shown. Scale bar, 50 μm. (**C**) Mean velocity, displacement, and meandering index of OT-$I^{GFP}$ $CD8^+$ T cells in HKx31-OVA-infected trachea. Points, individual cells pooled from three mice per each group. *$P < 0.001$ compared with IgG. Statistical differences in (**A** and **C**) were assessed with nonparametric Mann-Whitney test.

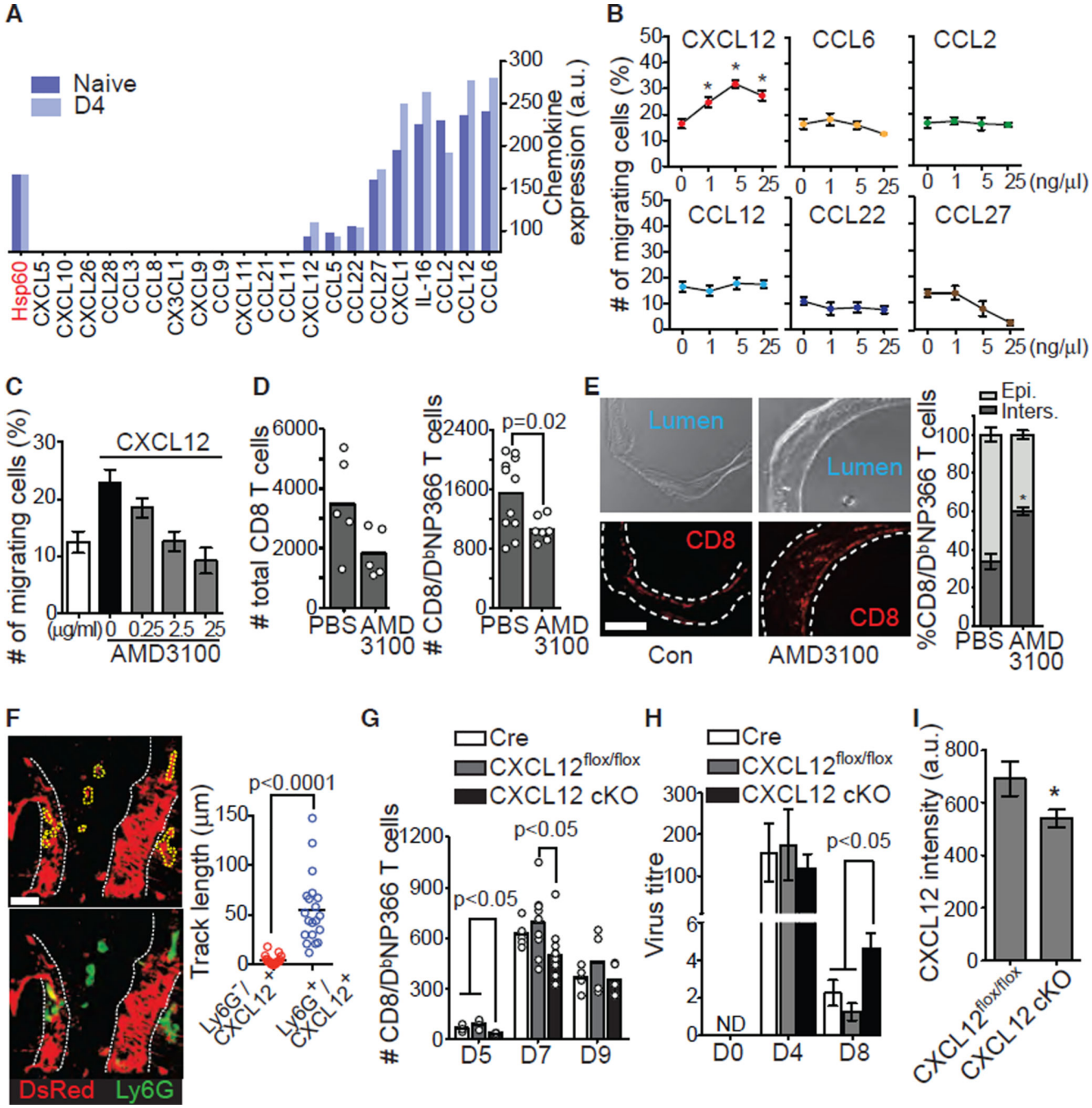


**Fig. 3. Neutrophil-derived CXCL12 induces CD8$^+$ T cell migration**

(**A**) Chemokine microarray with total lysates of bone marrow-derived neutrophils from naïve or influenza-infected mice at day 4 post-infection (*N* = 2 mice per group). Chemokine expression levels were expressed as an arbitrary unit measured by densitometry. (**B**) CD3/CD28-activated CD8$^+$ T cell migration on ICAM-1 with the indicated chemokines. The ratio of the number of cells crawling more than 50 μm for 15 min (% total) in a field of view was presented. A single assay analyzed at least 10 cells (*N* = 3 assays per group). **P* < 0.05 compared with Control. (**C**) CD8$^+$ T cell migration assay on ICAM-1 and CXCL12 in the

presence or absence of AMD3100, a CXCR4 antagonist ($N$ = 3 assays per group). (**D**) The number of total (left) or $D^bNP_{366}$-specific (right) $CD8^+$ T cells in the trachea at day 7 post-infection with or without AMD3100 ($N$ = 5 to 11 per group). (**E**) Immunofluorescent microscopy of tissue sections from the virus-infected trachea with or without AMD3100 treatment. Top, bright field images; bottom, $CD8^+$ T cells (red). The dotted lines indicate tracheal tissue borders. Graph, the ratio (% total) of $CD8^+$ T cell number in the epithelium and the interstitium ($N \geq 3$ sections per mouse, $N \geq 3$ mice per group, $^*P < 0.05$ compared with PBS). Scale bar, 250 μm. Epi., epithelium; Inters., interstitium. (**F**) Representative images from IV-TPM of $Ly6G^+DsRed^+$ neutrophils in the trachea of $CXCL12^{DsRed}$ mouse infected with influenza virus (Left, DsRed in red; Right, Ly6G in green + DsRed in red). White dotted line, blood vessel; yellow dotted area, neutrophil. Scale bar, 20 μm. Graph, track lengths of $Ly6G^-DsRed^+$ and $Ly6G^+DsRed^+$ cells for 15 min ($N$ = 3 mice per group). (**G**) Cre ($Ela2^{Cre/+}$), $CXCL12^{flox/flox}$, and CXCL12-cKO mice were infected and $D^bNP_{366}$-specific $CD8^+$ T cells in the trachea were measured by flow cytometry at the indicated days ($N$ = 3 to 8 per group). (**H**) Cre ($Ela2^{Cre/+}$), $CXCL12^{flox/flox}$, and CXCL12-cKO mice were infected and viral loads in the trachea were measured at the indicated days (% of CXCL12-cKO at day 4, $N$ = 4 to 8 per group). (**I**) Total CXCL12 intensity of the whole trachea tissue sections measured by fluorescent microscopy ($N \geq 3$ sections per mouse and $N$ = 6 mice per group, $^*P < 0.05$ compared with $CXCL12^{flox/flox}$). (**D, F,** and **G**) points indicate data from individual mice. (**B, G,** and **H**) were analyzed with Kruskal-Wallis followed by Dunn's post-test, (**D, E, F, G** (D7), and **I**) were analyzed with Student's t test.

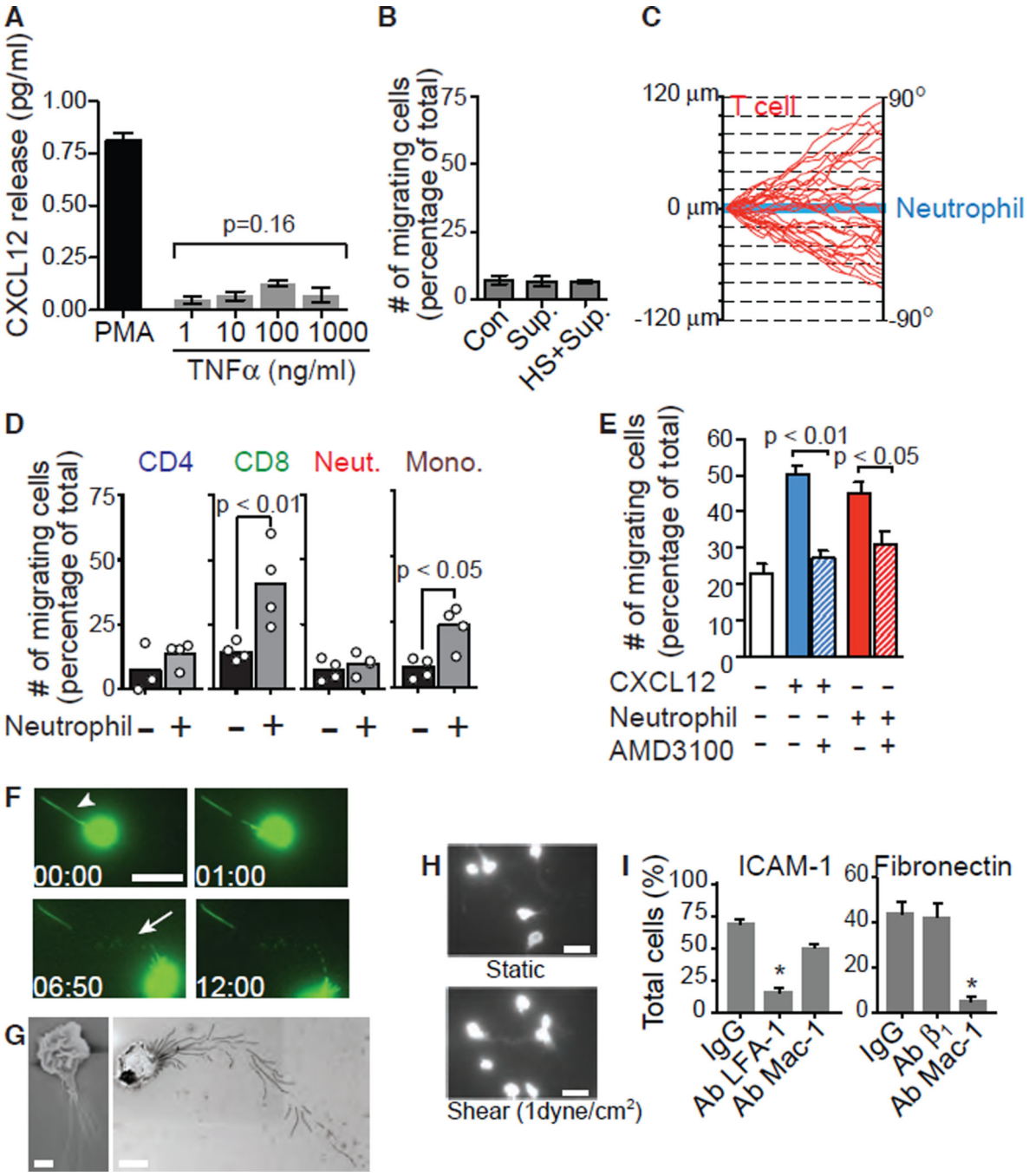


**Fig. 4. Neutrophil trails induce CD8$^+$ T cell migration**

(**A**) CXCL12 secretion from neutrophils in response to PMA (100 ng/ml) or the indicated concentration of TNFα ($N$ = 3). (**B**) Activated CD8$^+$ T cell migration on a chamber coated with ICAM-1 alone or with ICAM-1 + heparan sulfate (HS) pre-incubated with or without the supernatant from migrating neutrophils stimulated by fMLP ($N$ = 3). Sup., supernatant. (**C**) Tracking of single CD8$^+$ T cell migration (red) vs. neutrophil tracks (blue). The shortest distance of a CD8$^+$ T cell from a neutrophil track was measured at each time point of migration and plotted every 15 sec from t = 0 to t = 6 min (total 30 cells from three

independent assays). (**D**) Migration of indicated cells on neutrophilexperienced (+) or non-experienced (−) ICAM-1-coated surface. The ratio (% total) of cells migrating ≥ 50 μm ($CD4^+$, $CD8^+$, neutrophil) or ≥ 25 μm (monocyte) for 15 min in a field of view was presented. (**E**) CD3/CD28-activated $CD8^+$ T cell migration on ICAM-1 coated with CXCL12 or neutrophil trails in the presence or absence of AMD3100 ($N \geq 3$ assays per group). Points indicate data from individual experiments (average). (**F**) Time lapse images from a representative movie showing a Ly6G-stained (green) neutrophil crawling on ICAM-1 coated surface in the presence of fMLP. Arrowhead and arrow indicate neutrophil trails and $CD8^+$ T cell, respectively. Scale bars, 20 μm. (**G**) Scanning electron microscopy of neutrophil trails on ICAM-1. Scale bar, 2 μm (left) and 10 μm (right). (**H**) Immunofluorescence images of Ly6G-stained migrating neutrophils under a static condition or shear flow. Scale bars, 20 μm. (**I**) Integrin-dependent trail formation. Migrating neutrophils with trails were counted (% total) on ICAM-1 or fibronectin in the presence of the indicated blocking antibodies ($N = 3$ assays per group). *$P < 0.05$ compared with IgG. (**A**) was analyzed with Kruskal-Wallis followed by Dunn's post-test and (**D, E,** and **I**) were analyzed with Student's t test.

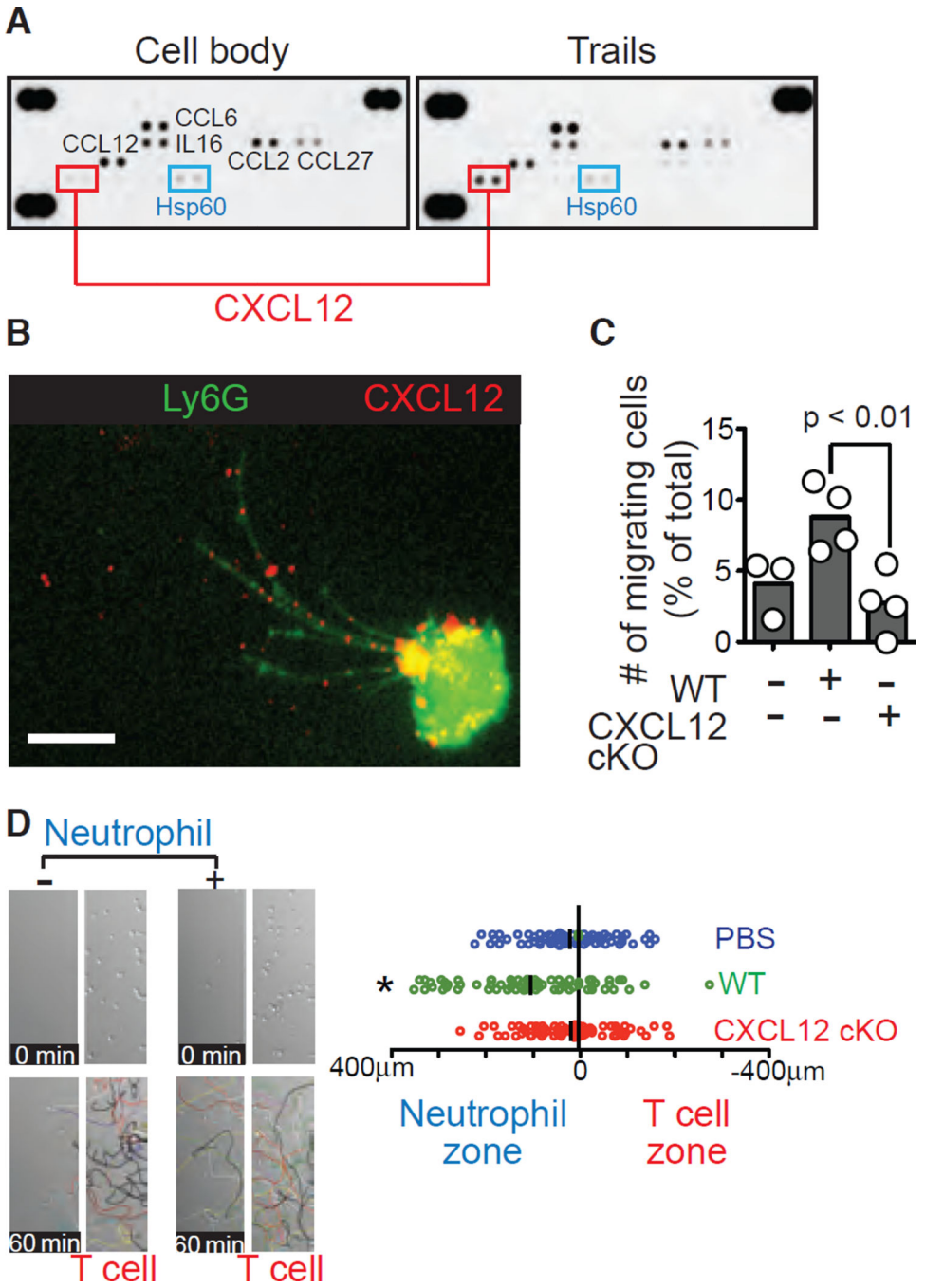


**Fig. 5. Neutrophil leaves CXCL12-containing trails**

(**A**) Chemokine microarray with lysates of neutrophil cell bodies or neutrophil trails. Signals at the three corners, pseudo-reactive reference spots; Hsp60, a loading control. (**B**) Immunofluorescence image of a migrating neutrophil stained with Abs against Ly6G (green) and CXCL12 (red). Scale bar, 20 μm. (**C**) Migration of activated $CD8^+$ T cells on ICAM-1 + trails generated by WT or CXCL12 cKO neutrophils. Points indicate data from individual experiments (average). (**D**) Activated $CD8^+$ T cell migration from “T cell zone” to “neutrophil zone” was tracked (top, t = 0 and bottom, t = 60min). Graph, the net

displacement values toward the empty zone (−) or the zone containing WT or CXCL12 cKO neutrophil trails (+). Individual cells pooled from three independent assays were plotted (lower panel). *$P < 0.0001$ compared with PBS & CXCL12 cKO. (**C**) was analyzed with nonparametric Mann-Whitney test and (**D**) was analyzed with Kruskal-Wallis followed by Dunn's post-test.

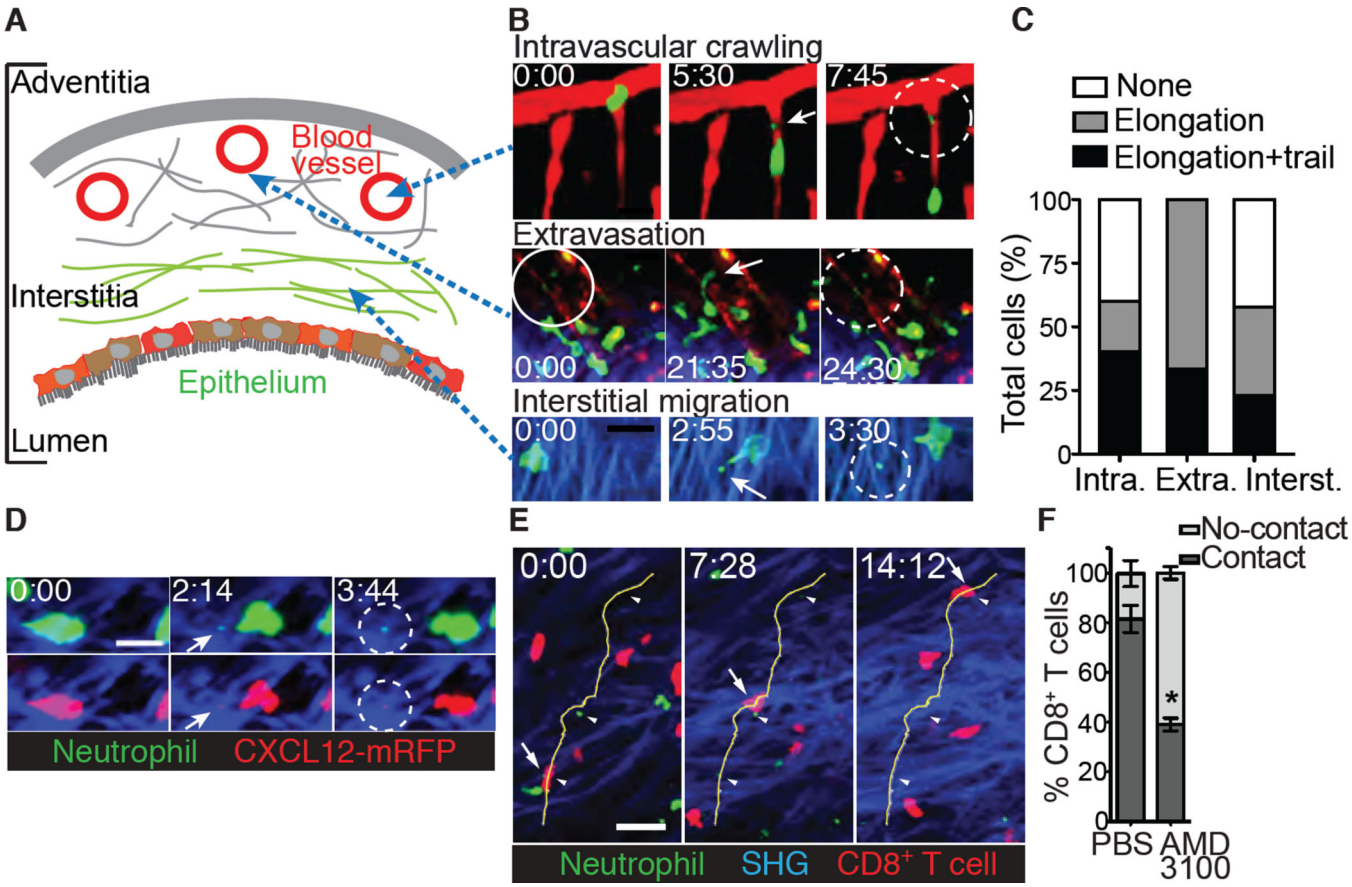


**Fig. 6. Neutrophils leave CXCL12-trails in the infected trachea**

(**A**) A cartoon illustrating trachea tissue structure. (**B**) Time lapse images from IV-TPM showing neutrophils migrating in the vessel (top), during extravasation (middle), and in the interstitial space (bottom) of the influenza-infected trachea. Green, Ly6G-stained neutrophils; Red, blood vessel (Texas red Dextran); Blue, SHG. White arrows and circles indicate trail formations. Scale bar, 25 μm. (**C**) Neutrophils were analyzed to quantify trail generation in the each step of migration including intravascular crawling (Intra.), extravasation (Extra.), and interstitial migration (Interst.). (**D**) Time lapse images from IV-TPM showing CXCL12+ trail generation during neutrophil migration in the mouse ear. Green, Gr1-stained neutrophils; Red, CXCL12-mRFP; Blue, SHG. White arrows and circles indicate trail formations. Scale bar, 20 μm. (**E**) Time lapse images from IV-TPM showing $CD8^+$ T cell migration following neutrophil trails. $CD8^+$ T cells (red) and neutrophils (green) were intradermally transferred to the mouse ear 3 hr prior to imaging. A representative of time lapse images was shown from 5 independent experiments. Blue, SHG. Scale bar, 30 μm. (**F**) The percentage of total $CD8^+$ T cells that make at least one contact with neutrophil trail during each imaging (> 20 min) was quantified. $CD8^+$ T cells were pretreated with or without AMD3100 prior to imaging ($N = 5$, $^*P < 0.01$ compared with PBS, Mann-Whitney test).

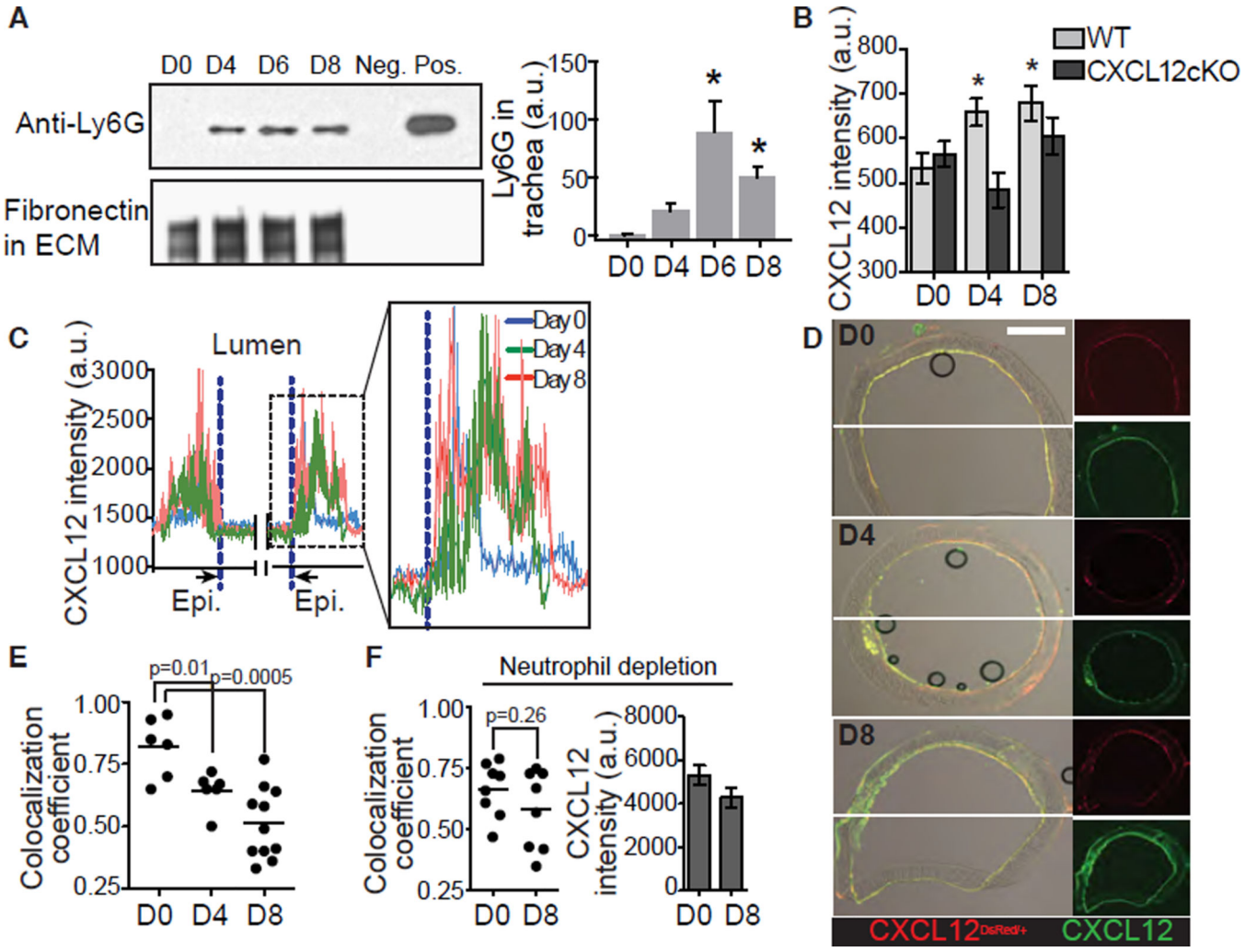


**Fig. 7. Expression of CXCL12 in the infected trachea depends on neutrophils trails**

(**A**) The presence of neutrophil-derived trails in the infected trachea was revealed by Western blot analysis with anti-Ly6G Ab. Supernatants from collagenase treated trachea were used after intact cells were removed. Negative control (Neg.), supernatants from collagenase-treated neutrophils. Positive control (Pos.), total neutrophil lysate. Graph, mean ± SEM. Ly6G intensity was normalized by fibronectin intensity ($N \geq 3$ mice per group, $^*P < 0.05$ compared with day 0 (D0)). (**B**) Trachea tissue sections from WT and CXCL12 were stained with CXCL12 antibody and the total intensity was measured from the entire tissue area. Graph, the mean fluorescent intensities (a.u./μm$^2$, mean ± SEM) of CXCL12 from each tissue section ($N \geq 2$ sections per mouse, $N = 3$ to 5 mice per group, $^*P < 0.05$ compared with D0). (**C**) CXCL12 line intensity profiles across the trachea were obtained (white lines in Fig. 7D) and plotted (Y-axis, CXCL12 intensity; X-axis, line distance; Epi, epithelium; mean ± SEM; $N \geq 2$ sections per mouse, $N = 3$ to 5 mice per group). (**D, E**) CXCL12 immunostaining (green) of CXCL12$^{DsRed}$ (red) trachea sections at the indicated days post-infection (D) and colocalization (Pearson's coefficient) of CXCL12 (green) and CXCL12$^{DsRed}$ cells (red) (E) ($N \geq 2$ sections per mouse, $N = 3$ mice per group). Scale bar, 200 μm. (**F**) Colocalization of CXCL12 (green) and CXCL12$^{DsRed}$ cells (red) (left), and the

total CXCL12 intensity (right) from the trachea sections at day 0 and 8 post-infection with or without neutrophil depletion ($N$ = 2 sections per mouse, $N$ = 4 mice per group). (**A** and **B**) were analyzed with Kruskal-Wallis followed by Dunn's post-test and (**E** and **F**) were analyzed with nonparametric Mann-Whitney test.